ELSEVIER

Advances in Engineering Software 32 (2001) 159–168

ADVANCES IN ENGINEERING SOFTWARE

www.elsevier.com/locate/advengsoft

Topology optimization of plate structures using a single- or three-layered artificial material model

F. Belblidia[a,b,*], J.E.B. Lee[a], S. Rechak[b], E. Hinton[a,✠]

[a]*Department of Civil Engineering, University of Wales, Swansea SA2 8PP, UK*
[b]*Département de Mécanique, Ecole Nationale Polytechnique, El-Harrach, B.P. 182, Algiers, Algeria*

Published in memory of Professor E. Hinton

Received 13 August 1999; accepted 1 May 2000

Abstract

This paper presents a topology optimization algorithm for Mindlin–Reissner plate structures. Single- and three-layered artificial material models are used with the resizing algorithm of Bendsøe and Kikuchi. The objective is to produce the stiffest single- or three-layered plate for a given volume by redistributing the material throughout the plate. Numerical examples are provided to illustrate the process.

Keywords: Topology optimization; Mindlin–Reissner plate theory; Plane stress models; Artificial material model

1. Introduction

The problem of finding optimum topologies for plate structures has been treated extensively in the literature. Since the late 1970s, it has been known that the optimum reinforcement of plates may include infinitely fine arrangements of ribs [1]. This has given a special motivation to the use of microscopically anisotropic plates using homogenization or other 'smear-out' techniques. Olhoff et al. [2] and Bendsøe [3] have investigated the optimum plate topology based on Kirchhoff's theory, while Bendsøe and Kikuchi [4], Soto and Dìaz [5] Suzuki and Kikuchi [6] have used the MR plate theory.

Three major techniques have been applied in structural topology optimization, they have some common aspects such as the material format used, the iterative improvement scheme used and the constraint satisfaction strategy. They can be classified as follows:

- Evolutionary methods (E) [7,8]: The basic idea of this method is to use the fully stressed design techniques. In this case the inefficient material is removed from the design domain to allow the emergence of a new topology. The removal process can be achieved by either varying the elastic modulus as a function of the strain energy density (as in the hard-kill/soft-kill methods) or by deleting from the design domain the space occupied by the group of elements with low strain energy density values (as done in the ESO technique).
- Homogenization methods (H) [9–11]: The material is represented by a sponge-like material with infinitely many micro-scale cells with void. The variation of the porosity of this material throughout the structure is optimized using an optimality criteria algorithm. Depending on the cell used, we have the rank-1, rank-2 or microcell material models which characterize the void size and orientation within the unit cell. A more engineering concept for this characterization is the artificial material model or the SIMP method.
- Hybrid methods (H/E) [12,13] which contain attributes of both (E) and (H) methods in differing degrees. The earliest model uses the concept of the Aboudi-cell method.

In the present paper, we consider the optimization of structures that can be accurately modelled in bending using Mindlin–Reissner (MR) models for lateral loading and plane stress models for in-plane loading. The objective is to find the stiffest plate structure subject to a given loading, boundary conditions and material

* Corresponding author. Address: Department of Civil Engineering, University of Wales, Swansea, UK.

0045-7949/01/$ - see front matter
PII: S0045-7949(00)00141-3

properties. The plate dimensions are constrained so that the plate fits within a specified thin box and has a specified weight.

Single- and three-layered finite element (FE) models are used. The stiffening topology (or layout) is found using a topology optimization algorithm based on the artificial material model or the SIMP method [10,11] with the resizing algorithm of Bendsøe and Kikuchi [4]. It is assumed that with the single-layered model, the material is removed creating zones of void and material within the layer. However, with the three-layered model, the middle layer must always be present throughout the whole plate during the optimization process. The material redistribution therefore takes place in the upper and lower layers. This results in an optimum stiffening topology, which is presented as a variable density plot for the stiffening layers.

The process of shape and/or sizing structural optimization can then continue, based on a fully integrated design optimization tool, FIDO, in order to produce a reliable design of the plate. Further details of the FIDO process can be found in Ref. [14].

2. Generalized Mindlin–Reissner plate theory

The main assumptions of MR plate theory, which allows for transverse shear deformation effects, are

- the displacements are small compared to the plate thickness,
- the stress normal to the plate mid-surface is negligible, and
- normals to the mid-surface remain straight but not necessarily normal to the mid-surface after deformation.

The plate displacements $\bar{u}$, $\bar{v}$ and $\bar{w}$ at any point (x,y,z) can be written as

$$\begin{aligned} &\bar{u}(x,y,z) = u(x,y) + z\theta_x(x,y), \\ &\bar{v}(x,y,z) = v(x,y) + z\theta_y(x,y), \qquad \bar{w}(x,y,z) = w(x,y), \end{aligned} \tag{1}$$

where $u(x,y)$, $v(x,y)$, $w(x,y)$, $\theta_x(x,y)$ and $\theta_y(x,y)$ are the weighted averages for the in-plane, transverse deflection and rotations of the normal in the xz-plane and the yz-plane, respectively.

Note that here we are using a more general version of the MR plate theory which allows membrane and bending behaviour.

The in-plane strains may be written as

$$\boldsymbol{\epsilon}_{\mathrm{p}} = \begin{bmatrix} \bar{u}_{,x} \\ \bar{v}_{,y} \\ \bar{v}_{,x} + \bar{u}_{,y} \end{bmatrix} = \begin{bmatrix} u_{,x} + z\theta_{x,x} \\ v_{,y} + z\theta_{y,y} \\ u_{,y} + v_{,x} + z(\theta_{x,y} + \theta_{y,x}) \end{bmatrix} = \boldsymbol{\epsilon}_{\mathrm{m}} + z\boldsymbol{\epsilon}_{\mathrm{f}}, \tag{2a}$$

$$\boldsymbol{\epsilon}_{\mathrm{sh}} = \begin{bmatrix} \bar{w}_{,x} + \bar{u}_{,z} \\ \bar{w}_{,y} + \bar{v}_{,z} \end{bmatrix} = \begin{bmatrix} w_{,x} + \theta_x \\ w_{,y} + \theta_y \end{bmatrix} = \boldsymbol{\epsilon}_{\mathrm{s}}, \tag{2b}$$

where $\boldsymbol{\epsilon}_{\mathrm{p}}$, $\boldsymbol{\epsilon}_{\mathrm{f}}$ and $\hat{\boldsymbol{\epsilon}}_{\mathrm{s}}$ are the membrane, curvature (or flexural) and transverse shear strains, and $\bar{u}_{,x} = \partial\bar{u}/x$. By assuming $\sigma_z = 0$, the stress–strain relations can be expressed in partitioned form as

$$\begin{bmatrix} \boldsymbol{\sigma}_{\mathrm{p}} \\ \boldsymbol{\sigma}_{\mathrm{sh}} \end{bmatrix} = \begin{bmatrix} \mathbf{D}_{\mathrm{p}} & \mathbf{0} \\ \mathbf{0} & \mathbf{D}_{\mathrm{sh}} \end{bmatrix} \begin{bmatrix} \boldsymbol{\epsilon}_{\mathrm{p}} \\ \boldsymbol{\epsilon}_{\mathrm{sh}} \end{bmatrix}, \tag{3}$$

where $\boldsymbol{\sigma}_{\mathrm{p}} = [\sigma_x, \sigma_y, \sigma_{xy}]^{\mathrm{T}}$ and $\boldsymbol{\sigma}_{\mathrm{sh}} = [\tau_{xz}, \tau_{yz}]^{\mathrm{T}}$, and for an isotropic material of elastic modulus E and Poisson's ratio ν

$$\mathbf{D}_{\mathrm{p}} = \frac{E}{1-\nu^2} \begin{bmatrix} 1 & \nu & 0 \\ \nu & 1 & 0 \\ 0 & 0 & (1-\nu)/2 \end{bmatrix} \quad \text{and} \quad \mathbf{D}_{\mathrm{sh}} = \frac{E}{2(1+\nu)} \begin{bmatrix} 1 & 0 \\ 0 & 1 \end{bmatrix}. \tag{4}$$

The strain energy may be rewritten as

$$\begin{aligned} W &= \frac{1}{2}\int_V [\boldsymbol{\epsilon}_{\mathrm{m}}^{\mathrm{T}} + z\boldsymbol{\epsilon}_{\mathrm{f}}^{\mathrm{T}}, \boldsymbol{\epsilon}_{\mathrm{sh}}^{\mathrm{T}}] \begin{bmatrix} \mathbf{D}_{\mathrm{p}} & \mathbf{0} \\ \mathbf{0} & \mathbf{D}_{\mathrm{sh}} \end{bmatrix} \begin{bmatrix} \boldsymbol{\epsilon}_{\mathrm{m}} + z\boldsymbol{\epsilon}_{\mathrm{f}} \\ \boldsymbol{\epsilon}_{\mathrm{sh}} \end{bmatrix} \mathrm{d}v \\ &= \frac{1}{2}\int_V \boldsymbol{\epsilon}_{\mathrm{m}}^{\mathrm{T}}\mathbf{D}_{\mathrm{p}}\boldsymbol{\epsilon}_{\mathrm{m}}\,\mathrm{d}v + \frac{1}{2}\int_V z\boldsymbol{\epsilon}_{\mathrm{f}}^{\mathrm{T}}\mathbf{D}_{\mathrm{p}}\boldsymbol{\epsilon}_{\mathrm{m}}\,\mathrm{d}v \\ &\quad + \frac{1}{2}\int_V \boldsymbol{\epsilon}_{\mathrm{m}}^{\mathrm{T}}\mathbf{D}_{\mathrm{p}}z\boldsymbol{\epsilon}_{\mathrm{f}}\,\mathrm{d}v + \frac{1}{2}\int_V z\boldsymbol{\epsilon}_{\mathrm{f}}^{\mathrm{T}}\mathbf{D}_{\mathrm{p}}z\boldsymbol{\epsilon}_{\mathrm{f}}\,\mathrm{d}v \\ &\quad + \frac{1}{2}\int_V \boldsymbol{\epsilon}_{\mathrm{s}}^{\mathrm{T}}\mathbf{D}_{\mathrm{sh}}\boldsymbol{\epsilon}_{\mathrm{s}}\,\mathrm{d}v. \end{aligned} \tag{5}$$

If we assume that the material in the plate is placed symmetrically about the mid-plane, there will be no membrane–fluxual coupling terms and then we have

$$\begin{aligned} W &= W_{\mathrm{m}} + W_{\mathrm{f}} + W_{\mathrm{s}} + \frac{1}{2}\int_A \boldsymbol{\epsilon}_{\mathrm{m}}^{\mathrm{T}}\mathbf{D}_{\mathrm{m}}\boldsymbol{\epsilon}_{\mathrm{m}}\,\mathrm{d}A \\ &\quad + \frac{1}{2}\int_A \boldsymbol{\epsilon}_{\mathrm{f}}^{\mathrm{T}}\mathbf{D}_{\mathrm{f}}\boldsymbol{\epsilon}_{\mathrm{f}}\,\mathrm{d}A + \frac{1}{2}\int_A \boldsymbol{\epsilon}_{\mathrm{s}}^{\mathrm{T}}\mathbf{D}_{\mathrm{s}}\boldsymbol{\epsilon}_{\mathrm{s}}\,\mathrm{d}A \end{aligned} \tag{6}$$

in which $\mathbf{D}_{\mathrm{m}}$, $\mathbf{D}_{\mathrm{f}}$ and $\mathbf{D}_{\mathrm{s}}$ are the matrices of membrane, flexural and transverse shear rigidities, respectively, and for a symmetric multi-layer model (with n layers) it may

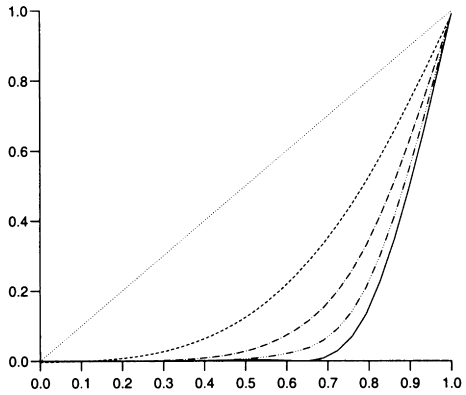

Fig. 1. Graph $\mathbf{D}^{\mathrm{h}}/\mathbf{D} = f(\Omega^{\gamma})$ for an artificial material with different value of γ. Legend: from left to right: $\gamma = 1$, 3, 5, 7 and 9.

be written as

$$\mathbf{D}_{\mathrm{m}} = \sum_{i=1}^{nl} \int_{z_i}^{z_{i+1}} \mathbf{D}_{\mathrm{p}_i}\, \mathrm{d}z, \qquad \mathbf{D}_{\mathrm{f}} = \sum_{i=1}^{nl} \int_{z_i}^{z_{i+1}} z^2 \mathbf{D}_{\mathrm{p}_i}\, \mathrm{d}z,$$
$$\mathbf{D}_{\mathrm{s}} = \sum_{i=1}^{nl} \int_{z_i}^{z_{i+1}} \frac{1}{\alpha} \mathbf{D}_{\mathrm{sh}_i}\, \mathrm{d}z, \tag{7}$$

where $\mathbf{D}_{\mathrm{p}_i}$ and $\mathbf{D}_{\mathrm{sh}_i}$ are the constitutive matrices for the ith layer and α is a shear modification factor.

Note that the associated stress resultant–strain resultant relationship may be written as

$$\begin{bmatrix} \boldsymbol{\sigma}_{\mathrm{m}} \\ \boldsymbol{\sigma}_{\mathrm{f}} \\ \boldsymbol{\sigma}_{\mathrm{s}} \end{bmatrix} = \begin{bmatrix} \mathbf{D}_{\mathrm{m}} & \mathbf{0} & \mathbf{0} \\ \mathbf{0} & \mathbf{D}_{\mathrm{f}} & \mathbf{0} \\ \mathbf{0} & \mathbf{0} & \mathbf{D}_{\mathrm{s}} \end{bmatrix} \begin{bmatrix} \boldsymbol{\epsilon}_{\mathrm{m}} \\ \boldsymbol{\epsilon}_{\mathrm{f}} \\ \boldsymbol{\epsilon}_{\mathrm{s}} \end{bmatrix} = \mathbf{D}\boldsymbol{\epsilon} \tag{8}$$

in which the membrane forces, the bending moment and the transverse shear forces are, respectively,

$$\boldsymbol{\sigma}_{\mathrm{m}} = [N_x, N_y, N_{xy}]^{\mathrm{T}} = \sum_{i=1}^{nl} \int_{z_i}^{z_{i+1}} [\sigma_x, \sigma_y, \tau_{xy}]^{\mathrm{T}}\, \mathrm{d}z,$$

$$\boldsymbol{\sigma}_{\mathrm{f}} = [M_x, M_y, M_{xy}]^{\mathrm{T}} = \sum_{i=1}^{nl} \int_{z_i}^{z_{i+1}} z[\sigma_x, \sigma_y, \tau_{xy}]^{\mathrm{T}}\, \mathrm{d}z, \tag{9}$$

$$\boldsymbol{\sigma}_{\mathrm{s}} = [Q_x, Q_y]^{\mathrm{T}} = \sum_{i=1}^{nl} \int_{z_i}^{z_{i+1}} [\tau_{xz}, \tau_{yz}]^{\mathrm{T}}\, \mathrm{d}z.$$

Normally in topology optimization with the three-layered model, the central layer is always taken as being solid whereas the upper and lower layers have equal constitutive properties that may represent a porous material. This is called the stiffening model. If the upper and lower layers are solid with the central layer representing a porous material then this is called a honeycomb model.

3. Artificial material model

The layered model is suitable for use as a structural representation when attempting to optimize the plate stiffening topology. In this representation, when dealing with a single-layer model, void and material zones are created within the plate. The value of the constitutive matrices $\mathbf{D}_{1\mathrm{m}}$ and $\mathbf{D}_{1\mathrm{s}}$ are therefore replaced by $\mathbf{D}^{\mathrm{h}}_{\mathrm{m}}$ and $\mathbf{D}^{\mathrm{h}}_{\mathrm{s}}$. The same procedure is applied to the three-layered stiffening model. However, here the values of the constitutive matrices $\mathbf{D}_{2\mathrm{m}}$, $\mathbf{D}_{3\mathrm{m}}$, and $\mathbf{D}_{2\mathrm{s}}$, $\mathbf{D}_{3\mathrm{s}}$ are replaced by $\mathbf{D}^{\mathrm{h}}_{\mathrm{m}}$ and $\mathbf{D}^{\mathrm{h}}_{\mathrm{s}}$ to represent the behaviour of the artificial material which is now described.

There are three main material models used in topology optimization: homogenized, rank-2 and artificial material models. The artificial material model, which is used in the present study, provides more practical structural layouts than the homogenized material model. In this model, instead of using the usual homogenized material model, the constitutive model can be expressed as

$$\mathbf{D}^{\mathrm{h}}_{\mathrm{m}} = \chi(\mathbf{x})\mathbf{D}_{\mathrm{m}} \qquad \text{and} \qquad \mathbf{D}^{\mathrm{h}}_{\mathrm{s}} = \chi(\mathbf{x})\mathbf{D}_{\mathrm{s}}, \tag{10}$$

where $\chi(\mathbf{x})$ is a discrete function which has the form

$$\chi(\mathbf{x}) = \begin{cases} 1 & \text{if } \mathbf{x} \in V_{\mathrm{s}} \quad \text{material} \\ 0 & \text{if } \mathbf{x} \notin V_{\mathrm{s}} \quad \text{no material} \end{cases} \tag{11}$$

For the numerical solution of the optimization problem, the discrete function χ causes solution difficulties [9]. One easy way to overcome these difficulties is to replace the discrete function χ by a continuous one ξ, where $0 \le \xi(\mathbf{x}) \le 1$. We will assume that the material has a micro-cellular structure and each cell is a square with a square hole of side length a, where $0 \le a \le 1$, and that the behaviour of the solid part of the structure is isotropic rather than truly orthotropic. There is, therefore, no dependency on the orientation of the square hole in the artificial material model unlike the case for the more conventional homogenized model. Thus in the present model

$$\xi(\mathbf{x}) = 1 - a^2(\mathbf{x}) \tag{12}$$

by using the material density parameter as a design variable $\varrho = (1 - a)$, the function may be written as

$$\xi(\mathbf{x}) = (2\varrho - \varrho^2). \tag{13}$$

The volume of solid material is then obtained by

$$V_s = \int_V \xi(\mathbf{x})\,dV = \int_V (2\varrho - \varrho^2)\,dV. \tag{14}$$

It is desirable to suppress the porous areas on the layer subject to optimization by penalizing its constitutive equations [10,11] by an exponent γ usually taken between 3 and 9. See Fig. 1 for an illustration of this relationship. This allows a better approximation to condition (11). Consequently, the rigidity matrices used in the stiffening layers can finally be expressed as

$$\mathbf{D}_m^h = (2\varrho - \varrho^2)^\gamma \mathbf{D}_m \qquad \text{and} \qquad \mathbf{D}_s^h = (2\varrho - \varrho^2)^\gamma \mathbf{D}_s. \tag{15}$$

4. Finite element analysis

A Lagrangian MR nine-node, general plate bending element with an associated nine-node overlayed plane stress element is adopted for the FE analysis in the topology optimization. The element has five degree of freedom (u, v, w, θ_x, θ_y) at each node and can be used for plate bending or plane stress by suppressing the appropriate degrees of freedom as required. The detailed fundamental formulation of the element can be found elsewhere [15].

As we will see later, as part of the optimizing process we will need the derivative of the strain energy with respect to the density parameter ϱ_i for each element i which will be composed of a unique material. To obtain a membrane–flexural energy dominant layout for the plate, and as the shear strain energy for thin plates is relatively small, only the derivative of the membrane and flexural strain energy W_{mf} has been taken into account here. Its derivatives with respect to the material density parameter ϱ_i are written as

$$\frac{\partial W}{\partial \varrho_i} \simeq \frac{\partial W_{mf}}{\partial \varrho_i} = \frac{\partial W_m}{\partial \varrho_i} + \frac{\partial W_f}{\partial \varrho_i} = \int_{A_i} \hat{\boldsymbol{\epsilon}}_m^T \frac{\partial \hat{\mathbf{D}}_m^h}{\partial \varrho_i} \hat{\boldsymbol{\epsilon}}_m + \int_{A_i} \hat{\boldsymbol{\epsilon}}_m^T \frac{\partial \hat{\mathbf{D}}_f^h}{\partial \varrho_i} \hat{\boldsymbol{\epsilon}}_m \, dA \tag{16}$$

where from Eq. (7)

$$\hat{\mathbf{D}}_m^h = (z_3 - z_2)\mathbf{D}_{1m} + (2\varrho - \varrho^2)^\gamma [(z_2 - z_1)\mathbf{D}_{2m} + (z_4 - z_3)\mathbf{D}_{3m}],$$

$$\hat{\mathbf{D}}_f^h = \frac{1}{3}(z_3^2 - z_2^3)\mathbf{D}_{1m} + \frac{(2\varrho - \varrho^2)^\gamma}{3}[(z_2^3 - z_1^3)\mathbf{D}_{2m} + (z_4^3 - z_3^3)\mathbf{D}_{3m}] \tag{17a}$$

for the three-layered model and

$$\hat{\mathbf{D}}_m^h = (2\varrho - \varrho^2)^\gamma (z_2 - z_1)\mathbf{D}_m, \qquad \hat{\mathbf{D}}_f^h = \frac{(2\varrho - \varrho^2)^\gamma}{3}(z_2^3 - z_1^3)\mathbf{D}_m \tag{17b}$$

for the single-layered model. Note that A_i is the area of element i.

In the examples presented later, the normalized value $W/W_{initial}$ is used to show the variation of the strain energy. Because we are dealing with the artificial material model, with a penalized form, the absolute strain energy value is therefore not exact.

5. Resizing algorithm

The resizing algorithm adopted in the topology optimization is now introduced. Each plate element is assumed to have stiffening layers: one layer for the single-layer model and the top and lower layers for the stiffening three-layer model. The layers with each element are composed of a unique artificial material with a unique density parameter ϱ. Here, we will simply provide an outline of the resizing algorithm, further details may be found elsewhere [4,6,9].

The topology optimization problem can be defined as follows: minimize the strain energy W_{mf}, such that the specified volume V_s must remain constant. The design variables are the material density parameters $\boldsymbol{\varrho} = [\varrho_1, \varrho_2, \ldots, \varrho_{nel}]$ where 'nel' is the number of elements.

The necessary optimality conditions for the material density parameters $\boldsymbol{\varrho}$ are a subset of the stationarity conditions of the Lagrangian function ($\mathscr{L}$) [9]

$$\mathscr{L}(\boldsymbol{\varrho}) = W_{mf} + \Lambda \sum_{i=1}^{nel} \left(\int_{V_i} (2\varrho_i - \varrho_i^2)\,dV - V_s \right) + \sum_{i=1}^{nel} \left(\int_{V_i} \lambda_{\varrho_i}^+ (\varrho_i - 1)\,dV - \int_{V_i} \lambda_{\varrho_i}^- \varrho_i \,dV \right), \tag{18}$$

where Λ, $\lambda_{\varrho_i}^+$ and $\lambda_{\varrho_i}^-$ are positive Lagrangian multipliers, W_{mf} the combined membrane and flexural strain energy of plate structure, and 'nel' the number of elements. The stationarity conditions for the material density ϱ_i are

$$\frac{\partial \mathscr{L}}{\partial \varrho_i} = \frac{\partial W_{mf}}{\partial \varrho_i} + 2\Lambda(1 - \varrho_i) + \lambda_{\varrho_i}^+ - \lambda_{\varrho_i}^- = 0, \qquad i = 1, \ldots, nel \tag{19}$$

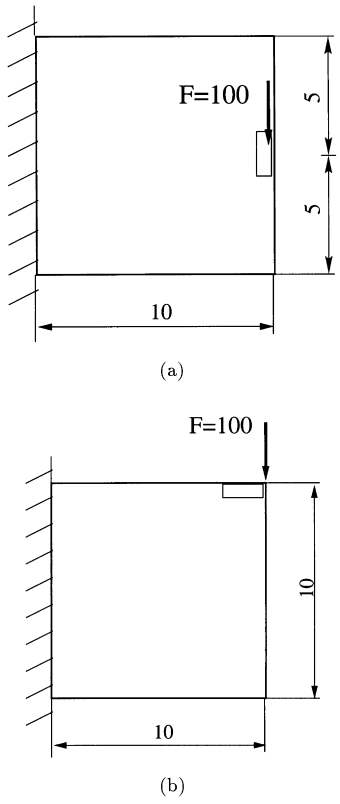

Fig. 2. Clamped at one edge square plate under: (a) load condition (i); (b) load condition (ii).

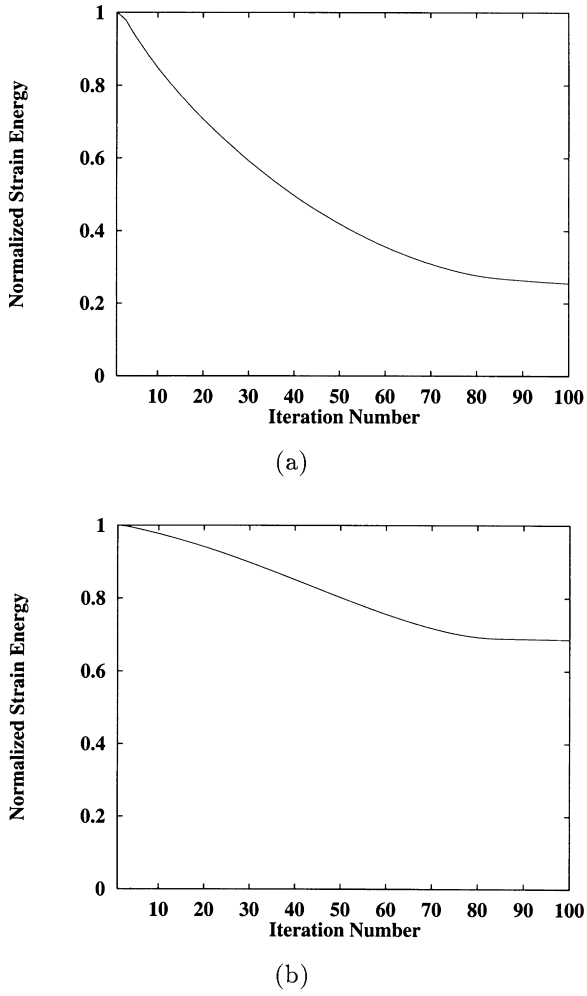

Fig. 3. Convergence of the normalized strain energy for clamped square plate under a point load at the right-hand edge (load condition (i)): (a) single-layer model; (b) three-layer model.

or,

$$\frac{\partial W_{\mathrm{mf}}}{\partial \varrho_i} = -2\Lambda(1-\varrho_i) - \lambda^{+}_{\varrho_i} + \lambda^{-}_{\varrho_i}, \qquad i = 1,\ldots,\mathrm{nel} \quad (20)$$

with the switching conditions

$$\lambda^{-}_{\varrho_i} \geq 0,\ \ \lambda^{+}_{\varrho_i} \geq 0,\ \ \lambda^{-}_{\varrho_i}\varrho_i \geq 0,\ \ \lambda^{+}_{\varrho_i}(\varrho_i - 1) \geq 0, \quad i = 1,\ldots,\mathrm{nel}. \quad (21)$$

For intermediate densities ($0 \leq \varrho_i \leq 1$) which means the side constraint is inactive, the necessary conditions can be rewritten as

$$\frac{1}{-2\Lambda(1-\varrho_i)}\frac{\partial W_{\mathrm{mf}}}{\partial \varrho_i} = 1, \qquad i = 1,\ldots,\mathrm{nel}. \quad (22)$$

A resizing algorithm can then be devised in the following form [9]:

$$\varrho_i^{k+1} = \begin{cases} \max\{(1-\zeta)\varrho_i^k, 1\} & \text{if } \varrho_i^k (B^k)^{\eta} \leq \max\{(1-\zeta)\varrho_i^k, 0\} \\ \varrho_i^k (B^k)^{\eta} & \text{if } \max\{(1-\zeta)\varrho_i^k, 0\} \leq \varrho_i^k (B^k)^{\eta} \leq \min\{(1+\zeta)\varrho_i^k, 1\} \\ \min\{(1+\zeta)\varrho_i^k, 0\} & \text{if } \min\{(1+\zeta)\varrho_i^k, 1\} \leq \varrho_i^k (B^k)^{\eta} \end{cases} \quad (23)$$

where

$$B^k = \frac{1}{2\Lambda(1-\varrho_i)}\frac{\partial W_{\mathrm{mf}}}{\partial_{\varrho_i}}, \qquad i = 1,\ldots,\mathrm{nel} \quad (24)$$

and η is a tuning parameter and ζ a moving limit. The subscript k implies the kth iteration in the resizing algorithm.

6. Topology optimization procedure

In topology optimization, the resizing algorithm and a FE

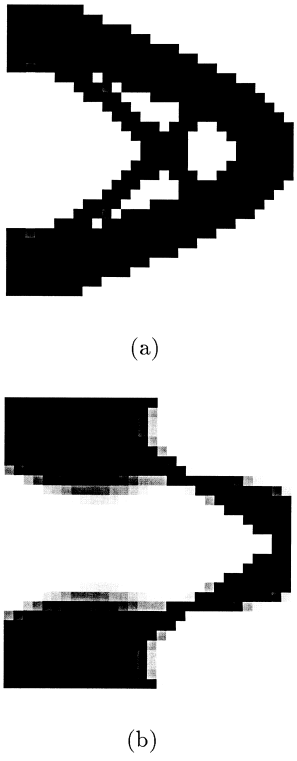

Fig. 4. Optimal stiffening topology for clamped square plate under a point load at the right-hand edge (load condition (i)): (a) single-layer model; (b) three-layer model.

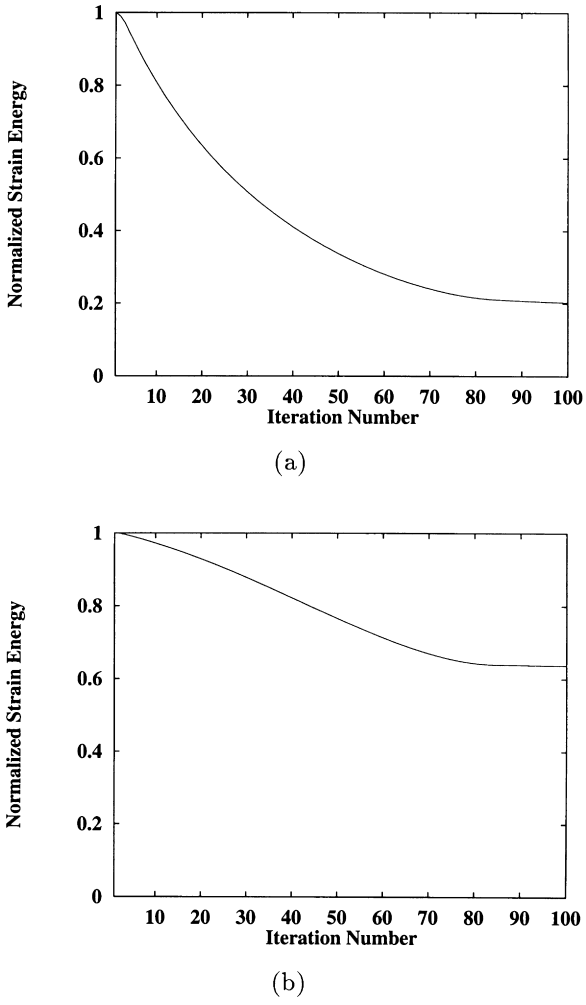

Fig. 5. Convergence of the normalized strain energy for clamped square plate under a point load at the top right-hand corner (load condition (ii)): (a) single-layer model; (b) three-layer model.

analysis using the artificial material are applied in each iteration step, and the original mesh does not change during the iteration process.

The volume of the structure is needed. The strain energy derivative is also required for each element i to update the material density parameter ϱ_i. Once the material density parameter for each element has been updated, a termination criterion is considered. If the termination criterion is satisfied, the topology optimization iteration is terminated.

The full topology optimization is now summarized:

1. Read problem data which includes: mesh data, boundary and loading conditions, material properties, definition of the design and non-design domains, required volume reduction, and solution parameters.
2. Before starting the topology optimization loop, initialize the density parameters ϱ_i for each element, and evaluate the rigidity matrices. Set the iteration parameter $k = 0$.
3. Increment the iteration number k by 1.
4. Perform a FE analysis for the current rigidity matrices.
5. Resize the density parameter ϱ_i within each element based on (23) and (24).
6. Check the optimization termination criterion: if this is satisfied then output the optimal density parameters and terminate the solution. Otherwise go to step (3).

Four termination criteria can be used:

- *The number of iterations:* a maximum number of iterations, $k_{\max}$, can be provided.
- *The strain energy norm:* the strain energy norm ($|W_k - W_{k-1}|/W_{k-1}$) between two subsequent topology optimization iterations may be examined and if it is smaller than a given value, then the program is terminated.
- *Strain energy level:* if the strain energy of the structure reaches a given value W_0, the solution is terminated.
- *Change of the density parameter:* if there is no further change in the density parameter, the solution is terminated.

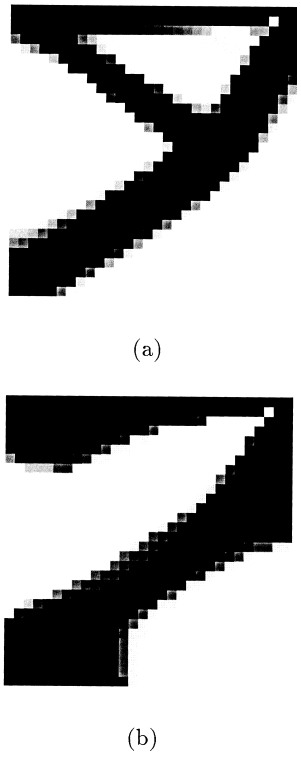

Fig. 6. Optimal stiffening topology for clamped square plate at one edge under a point load at the top right-hand corner (load condition (ii)): (a) single-layer model; (b) three-layer model.

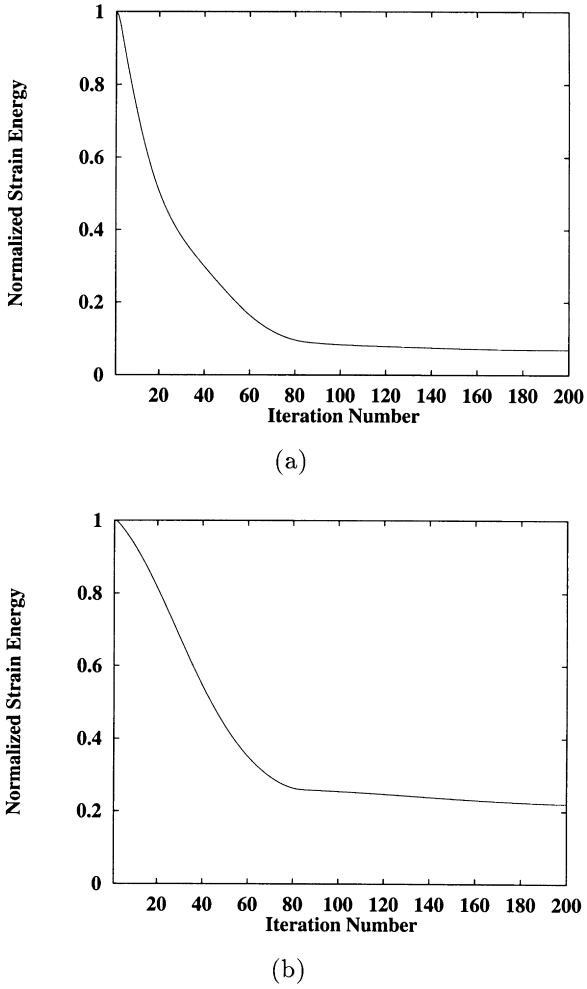

Fig. 7. Convergence of the normalized strain energy for simply supported square plate under a central point load: (a) single-layer model; (b) three-layer model.

7. Topology optimization examples

7.1. Introduction

The topology optimization is now illustrated for several problems involving membrane or bending behaviour. For each problem the variation of the normalized strain energy is presented with the material distribution history. Two material models are tested. The first one is the single-layer model where the layer is optimized by removing the material and creating two main zones. A dark zone (in the figures illustrating the results) represents the stiffening zone and the light zone represents void. The second model is the symmetric three-layered stiffening model with a solid central layer. This central layer remains solid during the optimization process and only the top and bottom layers are subject to optimization. The dark zone in the figures illustrating the results for this model indicates the existence of stiffening material in the top and bottom layers, while the light colour shows the existence of the central layer only.

7.2. Square plates subjected to in-plane loads

Fig. 2(a) and (b) shows square plates clamped on the left-hand edge and subjected to in-plane loadings for which optimal topologies are sought. We will investigate the optimal topologies using single- and three-layer models. The loading conditions are (i) a point load applied at the middle of the free edge opposite the clamped edge and (ii) a point load applied at the top right-hand corner. Note the non-design domain shown as a shaded region near the load in each case. No material may be removed in the non-design domain.

The FE analysis input data is: elastic modulus $E = 2.1 \times 10^5$, Poisson's ratio $\nu = 0.3$, load intensity (for both conditions) $F = -100$. A structured FE mesh consisting of 900 quadrilateral nine-node plane stress elements with 3721 nodes is used to represent the plate. The plate side length is $a = 10$, and the thickness is $h = 0.1$. For the three-layered model, the central solid layer thickness is $h_0 = 0.05$ and the combined top and bottom layers' thickness is $h_1 = 0.05$. All units are

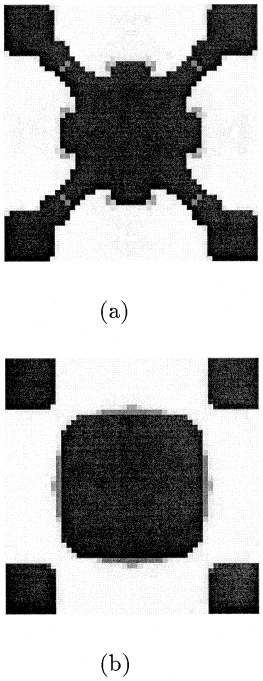

Fig. 8. Optimal stiffening topology for simply supported square plate under a central point load: (a) single-layer model; (b) three-layer model.

assumed to be consistent. For topology optimization, the input data quantities are: volume fraction $V_f = 50\%$, artificial material exponent $\gamma = 3$, tuning parameter $\eta = 1.0$, moving limit $\zeta = 0.015$ and volume constraint tolerance $\delta = 0.02$.

Fig. 3(a) and (b) illustrates the variation of the normalized strain energy with increasing number of iterations for the single- and three-layer plate model subjected to loading case (i).The optimal topologies for these plates are shown in Fig. 4(a) and (b) at 100 iterations.

Fig. 5(a) and (b) illustrates the variation of the normalized strain energy with increasing number of iterations for the single- and three-layer plate model subjected to loading case (ii). The optimal topologies for these plates are shown in Fig. 6(a) and (b) at 100 iterations.

7.3. Plates subjected to lateral loads

We now consider some plates subjected to lateral loads. In the two sets of examples the FE analysis input data is: elastic modulus $E = 10.92 \times 10^5$, Poisson's ratio $\nu = 0.3$, the load intensity $F = -100$, and the plate thickness $h = 0.1$. The topology optimization input data quantities are: volume fraction $V_f = 50\%$, artificial material exponent $\gamma = 5$, tuning parameter $\eta = 0.8$, moving limit $\zeta = 0.015$ and volume constraint tolerance $\delta = 0.001$. In all the examples

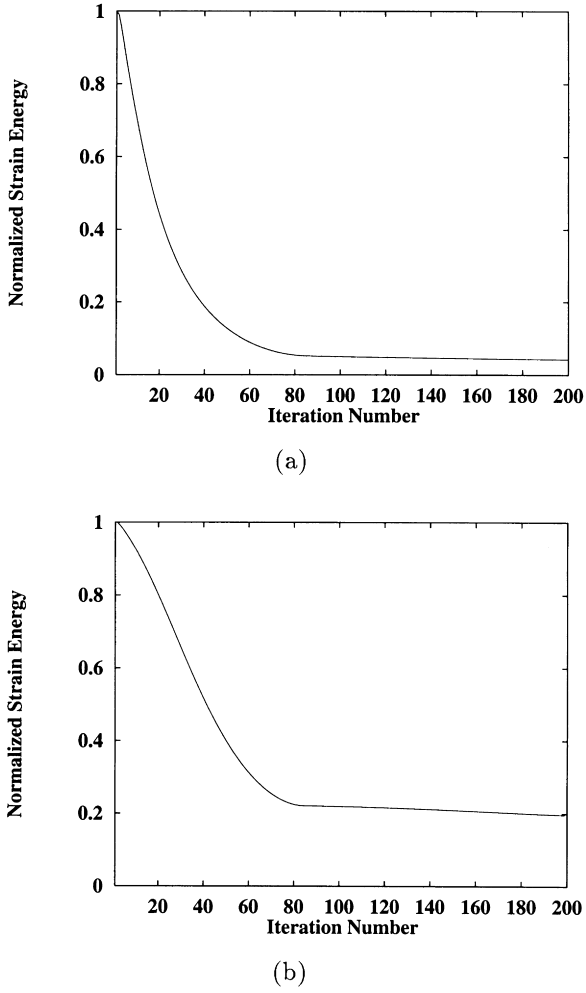

Fig. 9. Convergence of the normalized strain energy for clamped square plate under a central point load: (a) single-layer model; (b) three-layer model.

only a quadrant of the plate is analysed taking advantage of the symmetry and all units are assumed to be consistent.

7.3.1. Square plates under central load

The stiffening topologies for two centrally loaded square plates are optimized. They have the following sets of boundary conditions:

(i) S_e simply supported on all four edges, and
(ii) C_e clamped on all four edges.

A structured FE mesh consisting of 625 quadrilateral nine-node MR plate elements with 2601 nodes is used to idealize the plate quadrant, and the plate side length $a = 10$.

Fig. 7(a) and (b) illustrates the variation of the normalized strain energy with increasing number of iterations for the simply supported plate with a single layer and three layers,

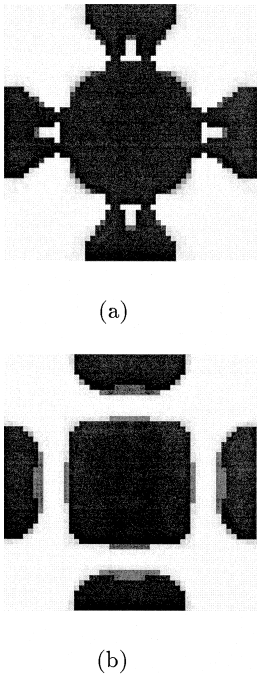

Fig. 10. Optimal stiffening topology for clamped square plate under a central point load: (a) single-layer model; (b) three-layer model.

respectively. The corresponding optimal topologies are shown in Fig. 8(a) and (b) at 200 iterations.

Fig. 9(a) and (b) illustrates the variation of the normalized strain energy with increasing number of iterations for the clamped plate with a single layer and three layers, respectively. The corresponding optimal topologies are shown in Fig. 10(a) and (b) at 200 iterations.

7.3.2. Simply supported square plate with a central circular hole subjected to four symmetrically placed point loads

The stiffening topology for the simply supported square plate shown in Fig. 11, with a central circular hole subjected to four symmetrically placed point loads, is optimized. A structured FE mesh consisting of 200 quadrilateral nine-node MR plate elements with 861 nodes is used to idealize the symmetric plate quadrant (see Fig. 11). The plate side length $a = 2$ and the radius of the hole is $R = 0.5$. Each load is located at the centre of each plate quadrant.

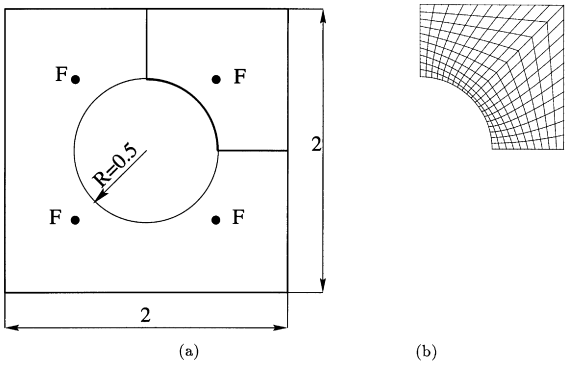

Fig. 11. Simply supported square plate with central circular hole subjected to four symmetrically placed point loads: (a) design domain; (b) mesh of plate quadrant.

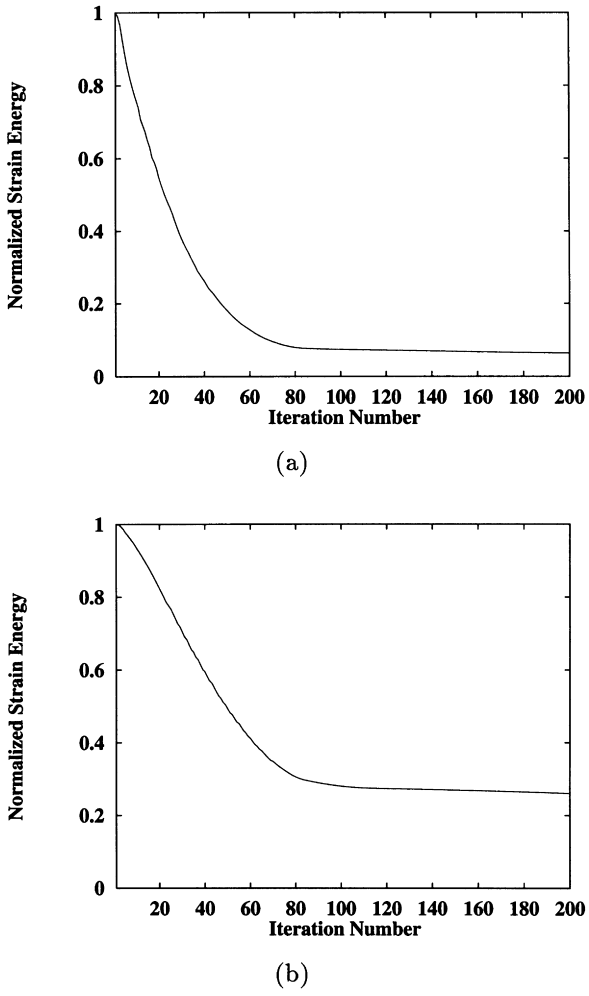

Fig. 12. Convergence of the normalized strain energy for simply supported square plate with central circular hole subjected to four point loads: (a) single-layer model; (b) three-layer model.

Fig. 12(a) and (b) illustrates the variation of the normalized strain energy with increasing number of iterations for the plate for a single- and three-layer model, respectively. The optimal topologies are shown in Fig. 13(a) and (b) at 200 iterations for the plate for the single- and three-layer models, respectively.

8. Conclusions

Using single- and three-layer, isotropic, nine-node plane stress and MR plate bending elements and a resizing

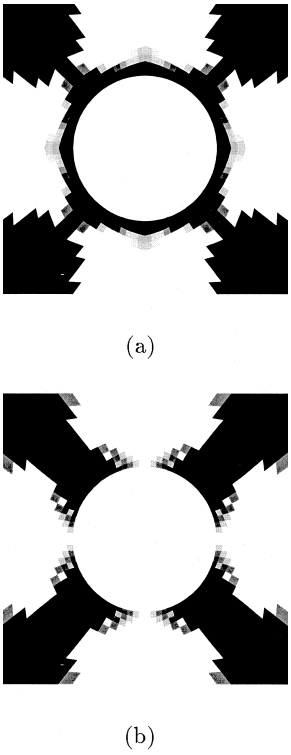

Fig. 13. Optimal stiffening topology for simply supported square plate with central circular hole subject to four symmetrically placed point loads: (a) single-layer model; (b) three-layer model.

algorithm, the topology optimization process has been illustrated using several numerical examples for plates under membrane and bending loading. In the examples studied, the material is re-distributed in order to minimize the strain energy with a constraint on the volume of the plate.

For plates under membrane behaviour there is a decrease of about 70–80% in the strain energy when using a single-layered model and about 30–35% when using a three-layered model. For plates under bending behaviour the strain energy decreases by about 80–90% for both models. The optimum design of plates is almost the same when using a single- or a three-layered model. However, the difference between a single- and three-layered model is more significant for plates under membrane behaviour where the solid central layer has a manifest structural purpose, while the design look remarkably alike for plates under bending behaviour.

Acknowledgements

The first author would like to thank the British Council (Algiers) for his sponsorship. The sponsorship of EPSRC grant "Fully Integrated Design Optimization of Engineering Structures (FIDO)" is also acknowledged.

Sadly during the correction of this paper Prof. E. Hinton passed away. He was a well respected man in the field of FE analysis and optimization and a good friend. He will be deeply missed by family, friends and colleagues.

References

[1] Cheng K-T, Olhoff N. An investigation concerning optimal design of solid elastic plates. Int J Solids Struct 1981;17:305–23.
[2] Olhoff N, Lurie KA, Cherkaev AV, Fedorov AV. Sliding regimes and anisotropy in optimal design of vibrating axisymmetric plates. Int J Solids Struct 1981;17:931–48.
[3] Bendsøe MP. Some smear-out models for integrally stiffened plates with applications to optimal design. In: Proc. Int. Symp. on Optimum Structural Design, University of Arizona, Tucson, Arizona, 1982. p. 13–34.
[4] Bendsøe MP, Kikuchi N. Generating optimal topologies in structural design using homogenization method. Comput Meth Appl Mech Engng 1988;71:197–224.
[5] Soto C, Dìaz A. On modeling of ribbed plates for shape optimization. Structural Optimization 1993;6:175–88.
[6] Suzuki K, Kikuchi N. A homogenization method for shape and topology optimization. Comput Meth Appl Mech Engng 1991;93:291–318.
[7] Xie YM, Steven GP. Evolutionary structural optimization. Berlin: Springer, 1997.
[8] Baumgartner A, Harzheim L, Mattheck C. SKO soft kill option. The biological way to find an optimum structure topology. Int J Fatigue 1992;14:387–93.
[9] Bendsøe MP. Optimization of structural topology shape and material. Berlin: Springer, 1995.
[10] Zhou M, Rozvany GIN. The COC algorithm, Part II: topological, geometrical and generalized shape optimization. Comput Meth Appl Mech Engng 1991;89:309–36.
[11] Rozvany GIN, Zhou M, Birker T. Generalized shape optimization without homogenization. Structural Optimization 1992;4:250–2.
[12] Paley M, Fuchs MB, Miroshnik E. The Aboudi micromechanical model for shape design of structures. In: Third Int. Conf. on Computational Structures Technology, Budapest, August 1996.
[13] Bulman S, Hinton E. Constrained adaptive topology optimization of engineering structures. Design Optimization 1999;1:419–39.
[14] Belblidia F. Fully integrated design optimization for plate structures. PhD thesis, Department of Civil Engineering, University of Wales, Swansea, 1999, C/Ph/231/99.
[15] Kanok-Nukulchai W. A simple and efficient finite element for general shell analysis. Int J Numer Meth Engng 1979;14:179–200.